Biocatalyst and continuous microfluidic reactor for an intensified production of *n*-butyl levulinate: kinetic model assessment

Alexandre Cordier[1], Marcel Klinksiek[3], Christoph Held[3], Julien Legros[1*], Sébastien Leveneur[2*]

[1]*INSA Rouen, CNRS, Normandie Université, UNIROUEN, COBRA laboratory, F-76000 Rouen, France, E-mail: julien.legros@univ-rouen.fr*

[2]*INSA Rouen, UNIROUEN, Normandie Univ, LSPC, UR4704, 76000 Rouen, France, E-mail: sebastien.leveneur@insa-rouen.fr*

[3] *Laboratory of Thermodynamics, Department of Biochemical and Chemical Engineering, TU Dortmund University, Emil-Figge. Str.70, 44227 Dortmund, Germany*

Abstract

The use of enzymes to catalyze chemical reactions has increased these recent years. Several models have been developed to express the kinetics over these biocatalysts. The most well-known of them, Michaelis-Menten, is used when only one substrate adsorbs on the enzyme. In the case of the esterification reaction, i.e., bimolecular system, a more complex kinetic model such as the Ping-Pong Bi-Bi should be applied. The use of such advanced models is essential for reactor scaleup and to optimize production. However, these models usually do not consider the reaction temperature. To fill this gap, a Ping-Pong Bi-Bi model was developed to produce butyl levulinate from the esterification of levulinic acid over an immobilized enzyme, Novozym®435. Microfluidic technology was used to ensure ideal mixing conditions. The Ping-Pong model, considering inhibition mechanisms, fits the experimental concentrations. ePC-SAFT equation of state was used to estimate the equilibrium constants.

Keywords

Kinetic modeling, ePC-SAFT, Enzyme, Ping-Pong mechanism

1. Introduction

Lignocellulosic biomass (LCB) is seen as the best alternative to fossil raw materials to make the chemical and fuel industries sustainable [1–3]. Compared to first-generation biomass, LCB is not competing with the food sector, avoiding the fuel versus food dilemma. The chemistry of this LCB valorization focuses on the production of platform molecules [4–6] and lignin valorization [4–6].

The platform molecule levulinic acid production has gained much interest these last years [7–9]. Levulinic acid or alkyl levulinates are starting materials for producing another platform molecule γ-valerolactone (GVL) [10–17]. Alkyl levulinates can be used directly as blending components for biodiesel or as a fuel oxygenate additives [18,19], and can also find applications as additives, solvents, and intermediates in fine chemistry [9]. In the study of Christensen et al., they showed that butyl levulinate (BL) improved conductivity, cold flow properties, and lubricity of diesel fuel and reduced its vapor pressure [20]. Moreover, it was found that BL remains in solution with diesel down to the fuel cloud point and has more compatibility with elastomers, compared to ethyl levulinate, which tends to separate from diesel at a temperature below 0 °C and results to be more corrosive [20]. Frigo et al., demonstrated that diesel fuel blended with a mixture of dibutyl ether and BL could reduce particulate emissions without changing engine power efficiency or increasing the NOx emission [21].

Alkyl levulinates can be produced via the alcoholysis of sugar monomers or LA esterification [7,8,22]. The latter route can be done via homogenous [23], heterogeneous [24–30] or enzymatic catalysis [31–37]. The use of heterogeneous catalysts such as resins, zeolite or immobilized enzymes should be favored to avoid additional separation stages [23]. From a chemical engineering viewpoint, using a continuous reactor for biomass valorization should be favored for large production [38].

Microreactor or microfluidic technology has raised interest in the scientific community because concentration and temperature gradients are reduced.

Production of n-butyl levulinate from LA esterification over lipase catalysis has been scarcely studied [32,34]. Yadav and Borkar [34] developed a kinetic model of LA esterification by butanol over Novozym®435, without considering the reversibility of this reaction or the temperature effect. Bhavsar and Yadav [34] showed that a continuous packed bed reactor with immobilized Novozym can be used to produce BL.

There is a need to intensify this reaction from an industrial [39] and fundamental standpoint. The use of a microreactor enables to operate in the absence of gradients allowing to use plug-flow model and thus simplifying the kinetic modeling stage [40]. The developed models proposed in the literature for the esterification of carboxylic acid over enzyme do not consider the temperature effect, and the knowledge of this effect on kinetic constants is mandatory for an industrial scaleup. In this manuscript, using microfluidic technology, kinetic models for the synthesis of BL over commercial Novozym®435 were developed and assessed at different temperatures.

2. Experimental section

2.1 Chemicals

All the chemicals were used as provided, without further purification. Butan-1-ol (wt% ≥ 99.9%), levulinic acid (wt% ≥ 99%), (trimethylsilyl)diazomethane (2.0 M in hexane) and the commercial supported *Candida Antarctica* lipase B (CAL-B), Novozym 435 (5000 $U.mg^{-1}$), were purchased from Sigma-Aldrich. Dichloromethane stabilized by ethanol was purchased from CARLO ERBA Reagents. Deionized water from the Aquadem™ system (Veolia) was used.

2.2 Analytical method

The aliquots taken at each residence time (t^R) for the analysis of butyl levulinate concentration were analyzed on a Thermo Scientific™ TRACE™ 1310 GC-FID equipped with an apolar column (DB-5MS, 30 m × 0.250 mm ID × 0.250 µm film thickness). The initial temperature of the analysis method was set at 50 °C for 2 min to reach 250 °C with a temperature rate of 25 °C/min. The aliquots were diluted in dichloromethane, and an excess of trimethylsilyl diazomethane as carboxylic acid scavenger was added (to protect the GC column from corrosion); 1 µL of the resulting solution was injected into the GC.

High field ^1H NMR analyses were performed on a 300 MHz Bruker Spectrospin spectrometer. Chemical shifts (δ) are given with regard to TMS using residual $CHCl_3$ solvent as an internal reference.

2.3 Procedure for the biocatalyzed esterification of levulinic acid with butanol in a flow reactor

The Luer-lock syringe, filled with levulinic acid, butanol and water, was connected to a preheating loop (PTFE tubing, ID = 1.59 mm, L = 126 cm) before the packed-bed reactor with an internal diameter of 6.6 mm. The packed-bed reactor was composed of an Omnifit^{TM} column filled with Novozym®435 immerged in a thermostated bath (Fig. 1).

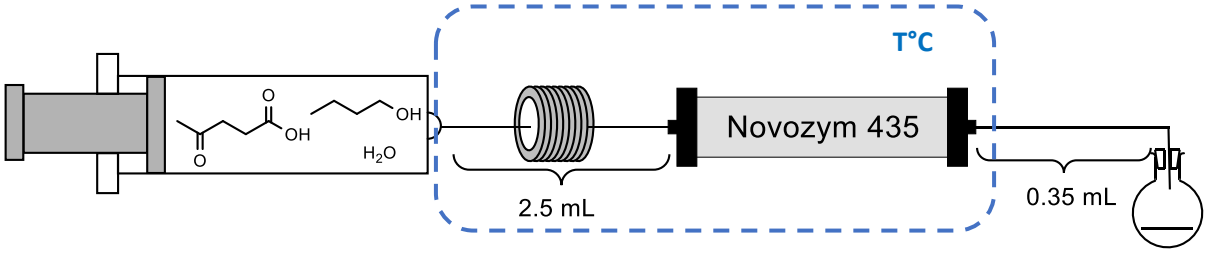

Fig.1. Process for the butyl levulinate synthesis with Omnifit cartridge.

The kinetic measurements were performed. First, the flow system was filled with the solution at a flow rate of 5 mL/min. Then the flow-rate was increased step by step to reach the desired t^R. The collection of aliquots began after running the system for 2 mL of reaction product collected, in order to reach the steady-state. The volume of the microreactor is related to the amount of the Novozym®435: 50 mg, 100 mg and 150 mg of supported CAL-B were packed 195 µL, 390 µL and 520 µL, respectively. The kinetic monitoring was performed as described in Table 1.

Table 1. Different flow-rates used for the kinetic monitoring.

Mass of Novozym®435 (mg) / Residence Time (min)	50 mg	100 mg	150 mg
30	6.5 µL/min	13 µL/min	17.33 µL/min
20	9.75 µL/min	19.5 µL/min	26 µL/min
15	13 µL/min	26 µL/min	34.66 µL/min
10	19.5 µL/min	39 µL/min	52 µL/min
7	27.85 µL/min	55.71 µL/min	74.28 µL/min
5	39 µL/min	78 µL/min	104 µL/min
3	65 µL/min	130 µL/min	173.33 µL/min
2	97.5 µL/min	195 µL/min	260 µL/min
1	195 µL/min	390 µL/min	520 µL/min
0	0 µL/min	0 µL/min	0 µL/min

Repeatability was assessed by collecting three samples after the steady-state, and it was found that the standard deviation was lower than 0.05 $mol.L^{-1}$. Furthermore, one run was repeated two times (Run 4) on different days to verify the repeatability of the whole system (Fig. S1.1). Fig. S1.1 shows that the repeatability is good.

Table 2 shows the experimental matrix used in this study.

123 Table 2. Experimental matrix for esterification.

Run	Temperature (°C)	Mass of catalyst (mg)	Void volume (µL)	Inlet (mol/L)				Ratio $[BuOH]_{in}/[LA]_{in}$
				BL	LA	BuOH	W	
1	20	100	390	0.00	2.61	7.81	0.34	3.00
2	35	100	390	0.00	2.61	7.81	0.34	3.00
3	50	100	390	0.00	2.61	7.81	0.34	3.00
4	65	100	390	0.00	2.61	7.82	0.34	3.00
5	80	100	390	0.00	2.61	7.81	0.34	3.00
6	65	150	520	0.00	2.61	7.81	0.34	2.99
7	65	50	195	0.00	2.61	7.81	0.34	2.99
8	65	100	390	0.00	5.09	5.09	0.31	1.00
9	50	100	390	0.00	5.16	5.16	0.32	1.00
10	35	100	390	0.00	5.09	5.09	0.31	1.00
11	20	100	390	0.00	5.09	5.09	0.31	1.00
12	65	150	520	0.00	5.09	5.09	0.31	1.00
13	65	50	195	0.00	5.09	5.09	0.31	1.00
14	65	100	390	0.00	1.74	8.71	0.32	4.99
15	50	100	390	0.00	1.77	8.83	0.33	5.00
16	35	100	390	0.00	1.79	8.95	0.33	4.99
17	20	100	390	0.00	1.82	9.07	0.34	4.99
18	65	50	195	0.00	1.74	8.71	0.32	4.99
19	65	150	520	0.00	1.74	8.71	0.32	4.99
20	65	100	390	0.00	2.59	7.76	0.70	3.00
21	50	100	390	0.00	2.59	7.76	0.70	3.00
22	35	100	390	0.00	2.59	7.76	0.70	3.00
23	20	100	390	0.00	2.59	7.76	0.70	3.00
24	65	100	390	0.00	2.46	7.78	1.20	3.17
25	50	100	390	0.00	2.57	7.69	1.20	3.00
26	35	100	390	0.00	2.46	7.78	1.20	3.17
27	20	100	390	0.00	2.46	7.78	1.20	3.17

124

125

2.4 Stability of Novozym 435

It is fundamental to evaluate the Novozym 435 stability to know if there are enzymes or another product leaching from support denaturation. Two experiments were performed: a degradability test for Novozym 435 in butanol solvent in a batch reactor and deactivation in the microfluidic system.

The degradability test was performed as follows: 100 mg of Novozym 435 were placed into 390 µL of a solution containing a $[BuOH]_{inlet}/[LA]_{inlet}$ ratio = 5. The mixture was heated at 65°C. After 1 h, the sample was filtered through a 30 µm PTFE frit of the Omnifit column (the exact same one that we used for the kinetic study), then $CDCl_3$ was added, and a ^1H NMR analysis was performed. The obtained spectrum was compared to those of authentic samples of butyl levulinate, n-butanol and levulinic acid, as well as those from PMMA and methyl methacrylate from the literature [41].

The deactivation test was carried out at 65 °C with 100 mg of catalyst and inlet levulinic acid concentration of 2.61 $mol.L^{-1}$. The outlet concentration of BL was followed with time-on-stream at 65°C.

3. Results

3.1 External and internal mass transfer evaluation

Besides the effect of mass transfer resistance on the kinetics, the presence or absence of flow maldistribution should be determined [42–44]. According to Doraiswamy and Tajbl [42], if the ratio reactor diameter on particle diameter is higher than 4, then they conclude that there is a proper liquid distribution with no channeling. In this system, this ratio is higher than 10. Thus, we concluded the absence of flow maldistribution.

To evaluate the influence of both effect, the same methodology presented by Leveneur et al. [45] was applied.

External mass transfer for each experiment was evaluated throughout the coefficient f_e (Equation (1)) defined by Villermaux [46]. If f_e is lower than 5%, then the external mass transfer is negligible.

$$f_e = \frac{\overline{r_{Obs}} \cdot L}{k_D \cdot C_b} \quad (1)$$

where, L is the ratio particle volume (V_P) on the external particle surface (A_P), $\overline{r_{Obs}}$ is the initial observed rate of esterification, k_D is the mass transfer coefficient and C_b the concentration in the bulk phase. In Equation (1), the concentration of LA in the bulk phase was used because butanol is in excess. The mean particle size of Novozym®435 is equal to 0.65 mm, and thus L is equal to $1.08 \cdot 10^{-4}$ m [47].

The mass transfer coefficient k_D can be estimated via the Sherwood number (Sh) expressed as

$$Sh = \frac{k_D \cdot \overline{d_P}}{D} = 2 + 1.8 \cdot Re_P^{\frac{1}{2}} \cdot Sc^{\frac{1}{3}} \quad (2)$$

where, d_P is the mean diameter of the catalyst particle, and Sc stands for the Schmidt number expressed as

$$Sc = \frac{\mu_f}{\rho_f \cdot D} \quad (3)$$

D is the molecular diffusion coefficient of LA in butanol calculated by the Wilke-Chang equation [48]. For instance, the molecular diffusion of LA in butanol at 50°C was found to be $9.02 \cdot 10^{-10}$ $m^2.s^{-1}$. The terms μ_f and ρ_f represent the viscosity and density of the fluid, i.e., butanol. These physicochemical properties were calculated from Ariba et al. work [49]. The f_e values were found to be lower than 5% for each experiment showing the absence of external mass transfer.

The internal mass transfer effect was evaluated via the Thieles modulus number ϕ_S defined by Equation (4) [46].

$$\phi_S^2 = \frac{\overline{r_{Obs}} \cdot L^2}{D_e . C_S} \quad (4)$$

If φ_S' is lower than 0.1, hence internal mass transfer can be assumed to be negligible. C_S is the LA concentration at the particle surface and in this study C_S=C_B because there is no external mass transfer. The term D_e represents the effective diffusion coefficient defined as $D_e = \frac{\varepsilon_P \cdot \sigma}{\tau} \cdot D$, where ε_P, σ and τ represent the porosity, constriction factor and tortuosity of the particle, respectively. From Ravelo et al. [47], Novozym®435 porosity is equal to 0.5. The tortuosity and constriction factor values were fixed to 6 and 1 [50]. Based on the φ_S' values of each experiment, the internal mass transfer can be assumed to be negligible.

3.2 Novozym 435 stability study

Novozym 435 degradability test (S2) is an essential study because its acrylic support/matrix tends to dissolve in many organic solvents [51–53]. By spectrum comparison of the mixture with a ^{1}H NMR analysis of different isolated products (butyl levulinate, n-butanol and levulinic acid), the mixture just contains n-butanol, levulinic acid and butyl levulinate and absolutely no traces of PMMA (or associate compound) were detected. Thus, our measurements are perfectly reliable with no interference from external chemicals.

Fig. 2 shows the BL concentration at the outlet versus time-on-stream. From Fig. 2, one can notice that enzyme deactivation can be neglected during the experiment.

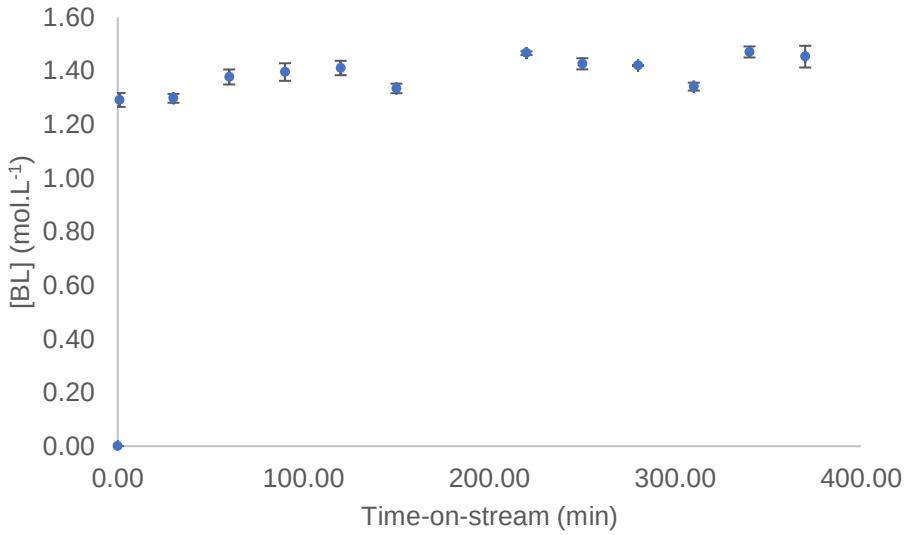

Fig. 2. Evolution of experimental BL concentration (blue circle) with error bars (black) versus time-on-stream at 65°C, $[LA]_{inlet}$=2.61 mol.L^{-1} and 100 mg of catalyst.

3.3 Temperature effect

Fig. 3 shows the effect of temperature on the ratio $\frac{[BL]}{[LA]_{inlet}}$, where [BL] is the experimental outlet concentration of BL. To evaluate this effect, experimental data

obtained from Runs 1-4 were compared, because there were carried out in the same operating conditions, except for the reaction temperature (Table 2). As expected, the kinetics of esterification increases with temperature.

These data can also be used to evaluate the effect of mass transfer. The natural logarithm of the initial rate constants versus 1/T was plotted (Fig. S3.1). From Fig. S3.1, the linearity between the natural logarithm of the initial rate constants and 1/T confirms the absence of mass transfer resistance.

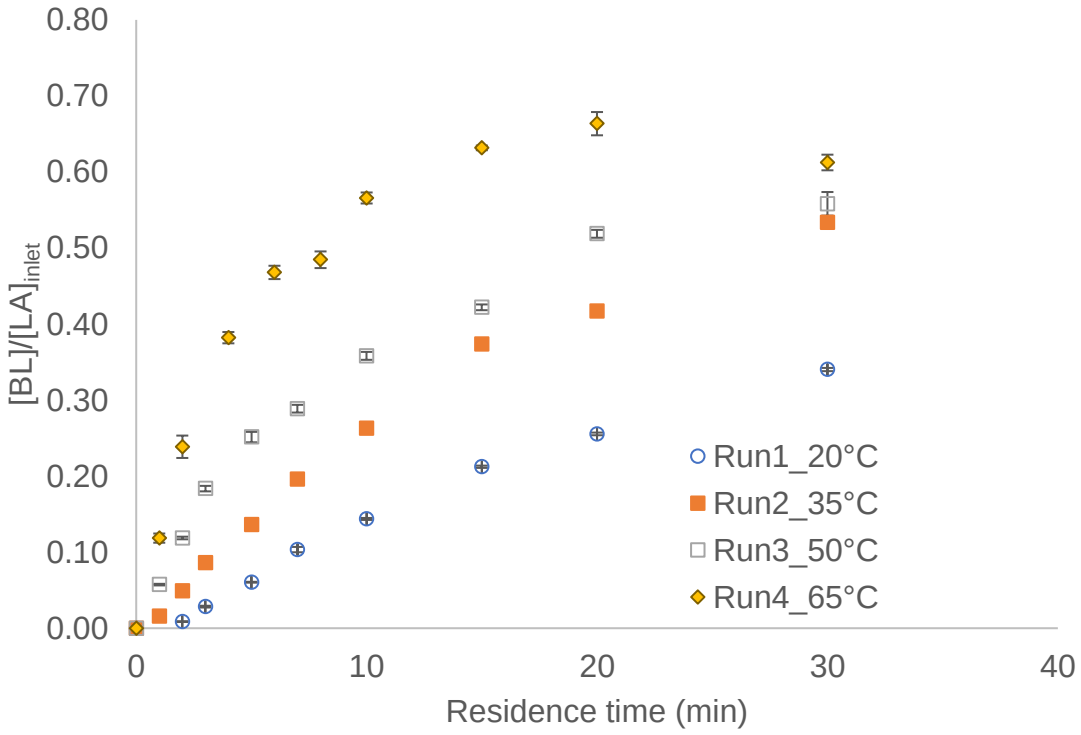

Fig.3. Effect of temperature on the experimental concentration ratio $[BL]/[LA]_{inlet}$ (Table 2): Run 1 at 20 °C (light blue circle), Run 2 at 35 °C (orange square), Run 3 at 50 °C (grey square), Run 4 at 65 °C (yellow diamond) and error bars (black).

3.4 Molar ratio effect

The effect of $\frac{[BuOH]_{inlet}}{[LA]_{inlet}}$ can affect the thermodynamics and kinetics of esterification [31]. Figs 4 and 5 show the effect of this ratio on the kinetics, via the normalized ratio $\frac{[BL]}{[LA]_{inlet}}$.

Different experiments carried out in similar operating conditions, except the ratio $\frac{[BuOH]_{inlet}}{[LA]_{inlet}}$, were compared (Table 2). One can notice that when $\frac{[BuOH]_{inlet}}{[LA]_{inlet}}$ is equal to 3:1 or 5:1, then the reaction rates and equilibrium values are similar. For a $\frac{[BuOH]_{inlet}}{[LA]_{inlet}}$ equal to 1:1, there is a deviation when the reaction reaches the equilibrium.

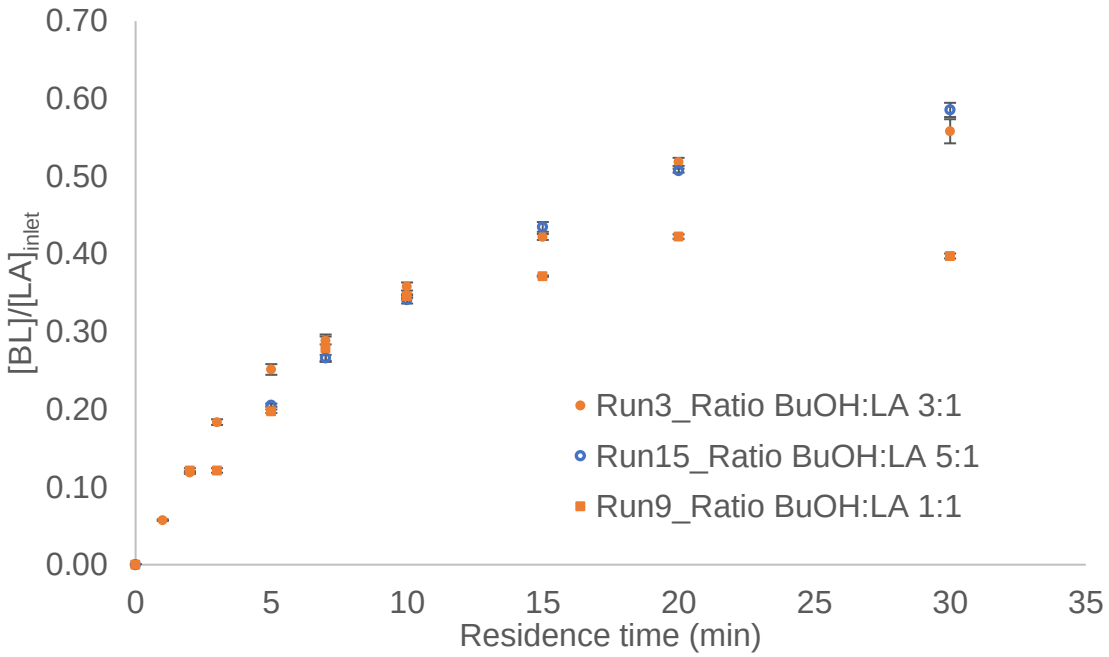

Fig.4. Effect of $\frac{[BuOH]_{inlet}}{[LA]_{inlet}}$ ratio on experimental concentration ratio $[BL]/[LA]_{inlet}$ at 50°C (Table 2): Run 3 at $\frac{[BuOH]_{inlet}}{[LA]_{inlet}} = 3:1$ (orange circle), Run 15 at $\frac{[BuOH]_{inlet}}{[LA]_{inlet}} = 5:1$ (blue circle), Run 9 at $\frac{[BuOH]_{inlet}}{[LA]_{inlet}} = 1:1$ (orange square) and error bars (black).

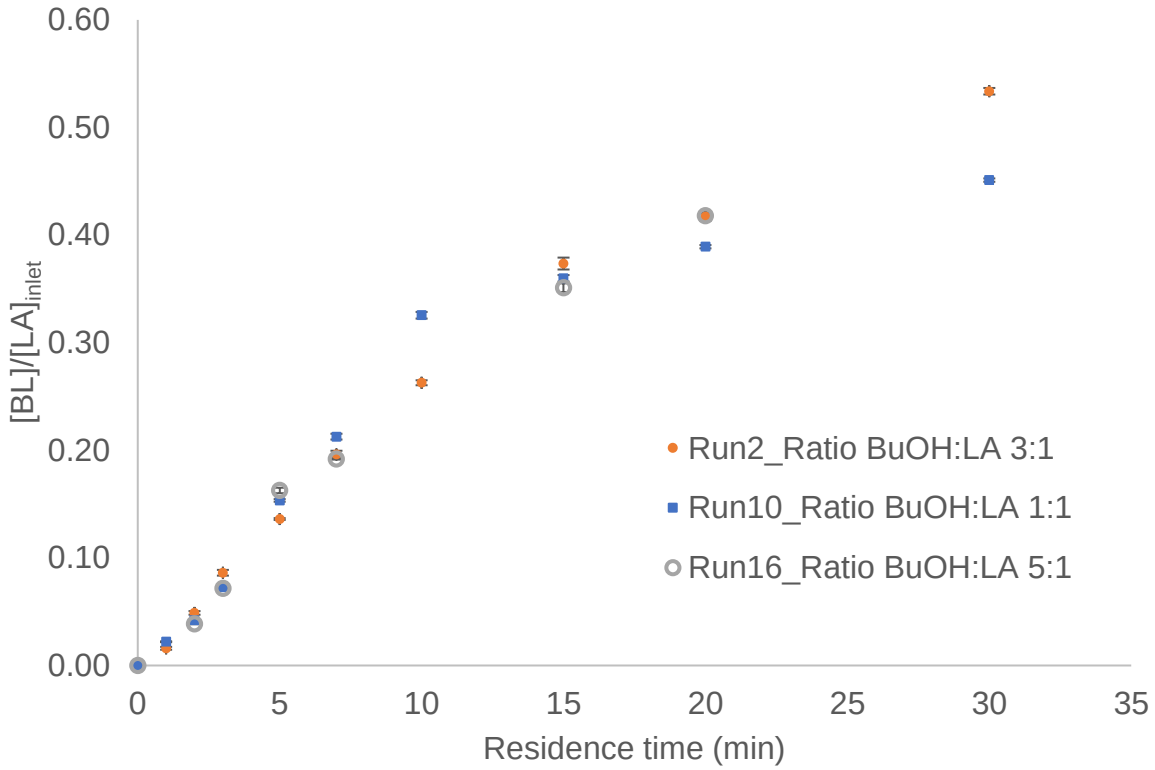

224

225 Fig.5. Effect of $\frac{[BuOH]_{inlet}}{[LA]_{inlet}}$ ratio on experimental concentration ratio [BL]/[LA]$_{inlet}$ at 35

226 °C (Table 2): Run 2 at $\frac{[BuOH]_{inlet}}{[LA]_{inlet}} = 3:1$ (orange circle), Run 10 at $\frac{[BuOH]_{inlet}}{[LA]_{inlet}} = 1:1$

227 (blue square), Run 16 at $\frac{[BuOH]_{inlet}}{[LA]_{inlet}} = 1:1$ (grey circle) and error bars (black).

228

3.5 Evaluation of equilibrium constant

The PC-SAFT equation of state first published by Gross and Sadowski [54] expresses the residual Helmholtz energy a^{res} as shown in Equation 5.

$$a^{res} = a^{hc} + a^{disp} + a^{assoc} \quad (5)$$

Thereby the hard-chain (a^{hc}) reference system represents the repulsive interactions between the molecules. The attractive interactions, such as the dispersion (a^{disp}), association (a^{assoc}), are described as perturbations of the reference system. More details on the modeling procedure and parameters used can be found in Supplementary Information (S4). Thermodynamic modeling of the reaction equilibrium is based on the temperature and pressure-dependent equilibrium constant K_{th}. It is calculated by the reacting agent concentrations in the equilibrium and activity coefficients according to Equation 6.

Based on Equation 5, we can calculate the temperature and pressure-dependent equilibrium constant K_{th}.

$$\mathrm{K_{th}(T,p) = K_{eq}(T,p,x) \cdot K_{\gamma}(T,p,x) = \prod_i (x_i \cdot \gamma_i)^{\nu_i}} \quad (6)$$

where, K_{eq} is determined from the experimental equilibrium concentrations and the activity coefficients are obtained by PC-SAFT [54–59]. The activity coefficient of each reactant *i* in the mixture is calculated from the ratio of the fugacity coefficients in the mixture and of the fugacity coefficient of the pure component.

$$\gamma_i = \frac{\varphi_i(T,p,x)}{\varphi_{0i}(T,p,x_i=1)} \quad (7)$$

The equilibrium constant K_{th} for each temperature enables the calculation of equilibrium concentrations at different conditions, i.e., molar ratios. The equilibrium

constant K_{th} was calculated based on the experiments with a molar ratio of BuOH:LA 3:1 (Table 3).

Table 3. Calculated equilibrium constant K_{th} based on the equilibrium concentrations of Runs 1-5 (Table 2).

T / °C	K_{eq}	K_{γ}	K_{th}
20	0.157	3.578	0.56
35	0.309	2.793	0.67*
50	0.356	2.308	0.82
65	0.491	1.969	0.97
80	0.695	1.732	1.20

*interpolated value

4. Discussion

4.1 Ping-Pong Models

Several authors showed that the Ping-Pong Bi-Bi mechanism can be used for the esterification reactions [32,60–66]. Several of them showed that alcohol and carboxylic acid can inhibit the enzyme, but none developed a kinetic model considering the reversibility of this reaction and the temperature effect on the kinetic constants.

Fig. 6 shows the Ping-Pong Bi-Bi mechanism for the esterification of LA by butanol.

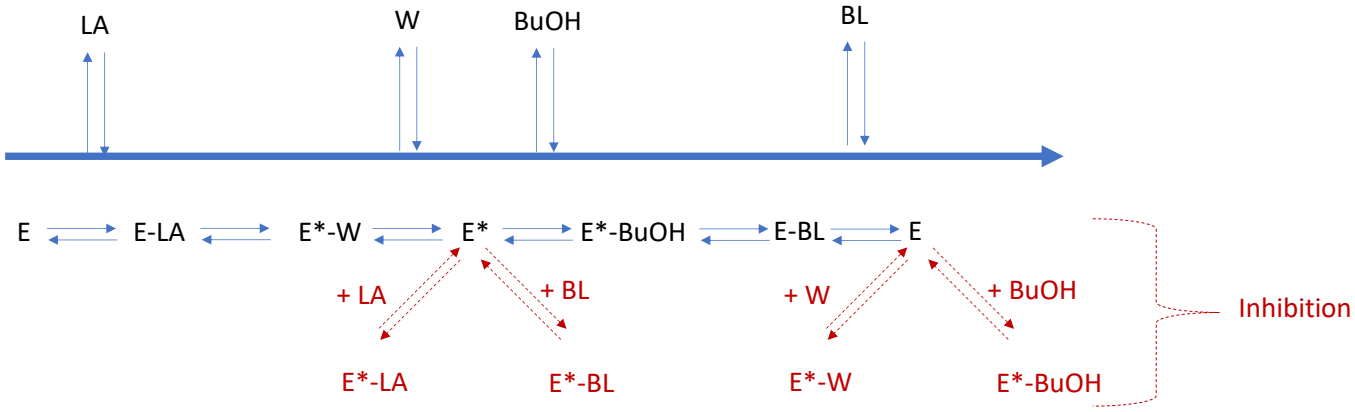

Fig. 6. Ping-Pong Bi-Bi and inhibition mechanism for the esterification of LA.

From Varma and Madras study [65], the rate equation can be derived as

$$r_{Esterification} = \frac{k_f \cdot k_b \cdot [E]_0^2 \cdot \left([LA] \cdot [BuOH] - \frac{[BL] \cdot [W]}{K_{eq}}\right)}{D} \quad (8)$$

where, $[LA]$, $[BuOH]$, $[BL]$ and $[W]$ are the outlet concentrations of levulinic acid, butanol, butyl levulinate and water, respectively. The term $[E]_0$ stands for the initial concentration of enzyme. The denominator D is expressed as

$$D = k_b \cdot [E]_0 \cdot [LA] \cdot [BuOH] + k_b \cdot [E]_0 \cdot K_{BuOH} \cdot [LA] \cdot \left(1 + \frac{[LA]}{K_{ILA}}\right)$$
$$+k_b \cdot [E]_0 \cdot K_{LA} \cdot [BuOH] \cdot \left(1 + \frac{[BuOH]}{K_{IBuOH}}\right) + \frac{k_f \cdot [E]_0 \cdot K_W}{K_{eq}} \cdot [BL] \cdot \left(1 + \frac{[BL]}{K_{IBL}}\right)$$
$$+ \frac{k_f \cdot [E]_0 \cdot K_{BL}}{K_{eq}} \cdot [W] \cdot \left(1 + \frac{[W]}{K_{IW}}\right)$$
$$+ \frac{k_f \cdot [E]_0}{K_{eq}} \cdot [W] \cdot [BL] + \frac{k_f \cdot K_{BL} \cdot [E]_0}{K_{IILA} \cdot K_{eq}} \cdot [W] \cdot [LA] + \frac{k_b \cdot K_{LA} \cdot [E]_0}{K_{IIBL}} \cdot [LA] \cdot [BL]$$
$$+ \frac{k_b \cdot K_{LA} \cdot [E]_0}{K_{BuOH-W}} \cdot [W] \cdot [BuOH] + \frac{k_b \cdot K_{BuOH} \cdot [E]_0}{K_{LA-BL}} \cdot [LA] \cdot [BL] \quad (9)$$

The terms $k_f \cdot [E]_0$ and $k_f \cdot [E]_0$ represent kinetic rate constants. The terms K_{LA}, K_{BL}, K_{BuOH} and K_W are the Michaelis constants for LA, BL, BuOH, and W, respectively. The inhibition constants by levulinic acid and BL are defined by K_{IILA} and K_{IIBL}. The dissociation constants, representing the dissociation of the inhibitor from the corresponding enzyme-inhibitor, are K_{ILA}, K_{IBL}, K_{IBuOH} and K_{IW}. The adsorption constants K_{BuOH-W} and K_{LA-BL} are lumped constants.

Mitchell and Krieger proposed a new rate expression of this Ping-Pong Bi-Bi mechanism [63],

$$r_{Esterification} = \frac{(k_{LA} \cdot [LA] \cdot k_{BuOH} \cdot [BuOH] - k_{BL} \cdot [BL] \cdot k_W \cdot [W]) \cdot [E]_0}{D'} \quad (10)$$

where, the denominator D' is

$$D' = k_{LA} \cdot [LA] \cdot \left(1 + \frac{[W]}{K_{IIW}} + \frac{[BuOH]}{K_{BuOH}}\right) + k_{BuOH} \cdot [BuOH] + k_W \cdot [W]$$
$$+k_{BL} \cdot [BL] \cdot \left(1 + \frac{[W]}{K_W} + \frac{[BuOH]}{K_{IIBuOH}}\right) \quad (11)$$

The terms k_{LA}, k_{BuOH}, $k_{BL}$and k_W are the specific constants of the enzyme for levulinic acid, butanol, butyl levulinate and water, respectively. K_{BuOH} and K_W are Michaelis-type constants for butanol and water, respectively. K_{IIBuOH} and K_{IIW} are the inhibition constants for butanol and water, respectively.

By considering the binding of BuOH or water with the free enzyme, D' becomes D''

$$D'' = k_{LA} \cdot [LA] \cdot \left(1 + \frac{[W]}{K_{IIW}} + \frac{[BuOH]}{K_{BuOH}}\right) + (k_{BuOH} \cdot [BuOH] + k_W \cdot [W]) \cdot \left(1 + \frac{[BuOH]}{K_{siBuOH}}\right) \cdot \left(1 + \frac{[W]}{K_{siW}}\right) + k_{BL} \cdot [BL] \cdot \left(1 + \frac{[W]}{K_W} + \frac{[BuOH]}{K_{IIBuOH}}\right) \quad (12)$$

where, K_{siBuOH} and K_{siW} stand for the constants between BuOH and water with the free enzyme.

According to Mitchell and Krieger [63], these equations are mathematically symmetric and less-lumped parameters. Different models were evaluated based on reaction rates developed by Mitchell and Krieger [63] and Varma and Madras [65].

4.2 Kinetic modeling

Experiments were performed in isothermal conditions, and internal and external mass transfers were found to be negligible. Plug-flow model was used; thus, material balances for each species can be written as

$$\frac{d[BL]}{d\tau} = r_{Esterification} \quad (13)$$

$$\frac{d[BuOH]}{d\tau} = -r_{Esterification} \quad (14)$$

$$\frac{d[LA]}{d\tau} = -r_{Esterification} \quad (15)$$

$$\frac{d[W]}{d\tau} = r_{Esterification} \quad (16)$$

where, τ is the space time defined as $\frac{V_L}{Q}$, V_L and Q are the volume of the liquid in the reactor and volumetric flow-rate, respectively.

Ordinary differential equations ODEs (13)-(16) were solved by the solver DDALPUS algorithm, via a damped Newton method [67].

For the non-linear regression, the concentration of BL was used as an observable. The estimation of the different kinetic constants (Equations (8)-(12)) was done via the minimization of the objective function $S(\theta)$ expressed as

$$S(\theta) = \sum_{u=1}^{n} w_u \cdot \left([BL]_{exp,u} - [BL]_{sim,u}\right)^2 = SSR \qquad (17)$$

where, w_u is the weigh factor for the experimental value *u*.

The objective function is expanded as a quadratic function of the parameters around the initial parameter values of the current iteration. The resulting quadratic minimization problem is solved with a modified Gauss-Jordan algorithm within a user-defined feasible region; then, a weak line search is conducted to establish an improved objective value and initial parameter vector for the next iteration. Interval estimates for the individual estimated parameters are then calculated from the final quadratic expansion of the objective function. This minimization is done by the package GREGPLUS to provide optimal parameter estimates with the 95% confidence intervals, expressed by the highest probability density (HPD). GREGPLUS provides the normalized parameter covariance matrix.

The GREGPLUS package and DDAPLUS solver are implemented in the Athena Visual Studio® 14.2 [68] used in this study.

Different models were evaluated based on the Ping-Pong Bi-Bi mechanism developed by the Varma and Madras study [65] and the Mitchell and Krieger study [63]. The term $[E]_0$was expressed by the catalyst loading ρ_{Enzyme}, i.e., the mass of catalyst divided by the volume of liquid in the reactor.

The general equation for esterification can be derived as

$$r_{Esterification} = k_{Esterification} \cdot \rho_{Enzyme} \cdot \frac{1}{D} \cdot \left([LA] \cdot [BuOH] - \frac{[BL] \cdot [W]}{K_{eq}} \right) \quad (18)$$

Different models were assessed, as summarized in Table 4.

Model 1 is the simplest one, by letting the denominator D equal to 1.

Models 2-4 are derived from Varma and Madras. Equation (8) was divided by k_b.To ease the parameter estimation and avoid division by very low number (close to zero) or high number, the following modification were included

$$K''_{ILA} = \frac{K_{BuOH}}{K_{ILA}}, K''_{IBuOH} = \frac{K_{LA}}{K_{IBuOH}}, K''_W = \frac{K_W}{K_{eq}}, K''_{BL} = \frac{K_{BL}}{K_{eq}}, K''_{IBL} = \frac{K''_W}{K_{IBL}}, K'_W = k_f \cdot K_W \cdot \frac{1}{k_b} \cdot \frac{1}{K_{eq}},$$

$$K''_{IW} = \frac{K''_{BL}}{K_{IW}},$$

$$K'_{BL} = k_f \cdot K_{BL} \cdot \frac{1}{k_b} \cdot \frac{1}{K_{eq}}$$

$$K_{Lump} = \frac{k_f}{k_b \cdot K_{eq}}, K''_{IIBL} = \frac{K_{LA}}{K_{IIBL}}, K''_{BuOH-W} = \frac{K_{LA}}{K_{BuOH-W}} \; and \; K''_{LA-BL} = \frac{K_{BuOH}}{K_{LA-BL}}$$

Model 2 ignores the inhibition mechanism, hence K''_{ILA}, K''_{IBL}, K''_{IW}, K''_{IBuOH}, K''_{IILA}, K''_{IIBL}, K''_{LA-BL}, and K''_{BuOH-W} were fixed to zero.

Model 3 considers the inhibition by butanol and ignores the other inhibition mechanism, hence K''_{ILA}, K''_{IBL}, K''_{IW}, K''_{IILA}, K''_{IIBL}, K''_{LA-BL}, and K''_{BuOH-W} were fixed to zero.

Model 4 considers all inhibition mechanisms.

Models 5-6 are derived from Mitchell and Krieger.

Model 5 is based on Equation (10) and Equation (11) divided by k_{BuOH}. The following notations are used

$$K_{eq} = \frac{k_{LA} \cdot k_{BuOH}}{k_{BL} \cdot k_W}, K_1 = \frac{k_{LA}}{k_{BuOH}}, K_2 = \frac{k_W}{k_{BuOH}}, K_3 = \frac{k_{BL}}{k_{BuOH}}, K''_{IBuOH} = \frac{1}{K_{IBuOH}}, K''_W = \frac{1}{K_W},$$
$$K''_{BuOH} = \frac{1}{K_{BuOH}}, K''_{IW} = \frac{1}{K_{IW}}, K''_{BuOH-W} = \frac{1}{K_{BuOH-W}} \; and \; K''_{LA-BL} = \frac{1}{K_{LA-BL}}$$

Model 6 is based on Equation (10) and divided Equation (12) by k_{BuOH}. The following notations are included

$$K''_{siBuOH} = \frac{1}{K_{siBuOH}} \; and \; K''_{siW} = \frac{1}{K_{siW}} \tag{19}$$

Table 4. Kinetic models tested in this study.

Model	Kinetic term	Denominator
Model 1	$k_{Esterification} \cdot \rho_{Enzyme}$	1
Model 2	$k_f \cdot \rho_{Enzyme}$	$[LA] \cdot [BuOH] + K_{BuOH} \cdot [LA] + K_{LA} \cdot [BuOH] + K''_W \cdot [BL] + K''_{BL} \cdot [W] + K_{Lump} \cdot [W] \cdot [BL]$
Model 3	$k_f \cdot \rho_{Enzyme}$	$[LA] \cdot [BuOH] + K_{BuOH} \cdot [LA] + K_{LA} \cdot [BuOH] + K''_{IBuOH} \cdot [BuOH]^2 + K''_W \cdot [BL] + K''_{BL} \cdot [W] + K_{Lump} \cdot [W] \cdot [BL]$

Model 4	$k_f \cdot \rho_{Enzyme}$	$[LA] \cdot [BuOH] + K_{BuOH} \cdot [LA] + K''_{ILA} \cdot [LA]^2$ $+K_{LA} \cdot [BuOH] + K''_{IBuOH} \cdot [BuOH]^2$ $+K''_W \cdot [BL] + K'_{IBL} \cdot [BL]^2$ $+K''_{BL} \cdot [W] + K''_{IW} \cdot [W]^2$ $+K_{Lump} \cdot [W] \cdot [BL] + K'''_{IILA} \cdot [W] \cdot [LA]$ $+K'''_{IIBL} \cdot [LA] \cdot [BL]$ $+K''_{BuOH-W} \cdot [W] \cdot [BuOH]$ $+K''_{LA-BL} \cdot [LA] \cdot [BL]$
Model 5	$k_{LA} \cdot \rho_{Enzyme}$	$K_1 \cdot [LA] + K''_{IW} \cdot [W] \cdot [LA] + K''_{BuOH} \cdot [BuOH] \cdot [LA]$ $+[BuOH] + K_2 \cdot [W]$ $+K_3 \cdot [BL] + K'_W \cdot [W] \cdot [BL] + K'_{IBuOH} \cdot [BuOH] \cdot [BL]$
Model 6	$k_{LA} \cdot \rho_{Enzyme}$	$K_1 \cdot [LA] + K''_{IW} \cdot [W] \cdot [LA] + K''_{BuOH} \cdot [BuOH] \cdot [LA]$ $+([BuOH] + K_2 \cdot [W]) \cdot (1 + K''_{siBuOH} \cdot [BuOH])$ $\cdot (1 + K''_{siW} \cdot [W])$ $+K_3 \cdot [BL] + K'_W \cdot [W] \cdot [BL] + K'_{IBuOH} \cdot [BuOH] \cdot [BL]$

To decrease the correlation between the pre-exponential factor and activation energy and ease the parameter estimation stage, the following modified Arrhenius equation was used [69].

$$k_c(T) = exp\left[ln\left(k_c(T_{ref})\right) + \frac{E_a}{R \cdot T_{ref}} \cdot \left(1 - \frac{T_{ref}}{T}\right)\right] \quad (20)$$

where, T_{ref} is a reference temperature which is the average temperature of the experimental matrix (Table 1).

The following constants were estimated: $ln\left(k_c\left(T_{ref}\right)\right)$, $\frac{E_a}{R \cdot T_{ref}}$, Michaelis-Menten and inhibition constants. Michaelis-Menten and inhibition constants were assumed to be temperature independent.

The effect of the number of estimated parameters on the models was evaluated via the AIC number standing for Akaike Information Criterion [16,17,70].

$$AIC = Number\ of\ independant\ event \cdot ln\left(\frac{SSR}{number\ of\ independant\ event}\right) + 2 \cdot Number\ of\ estimated\ parameters \quad (21)$$

4.3 Modeling results

In the first step, preliminary modeling results showed that some parameters tend to zero. Thus, these parameters were discarded:

-For Model 2, K''_W, K_{Lump} and K''_{BL} were discarded in the modeling.

-For Model 3, K_{LA}, K''_W and K''_{BL} were not considered.

-For Model 4, K_{BuOH}, K_{LA}, K''_W, K''_{BL}, K_{Lump}, K'''_{IILA}, K'_{IBL}, K''_{IW} and K'''_{IBL} and K''_{LA-BL} were neglected.

-For Model 5, K''_W, K''_{IW}, K_1, K_2, K'_{IBuOH} and K_3 were neglected.

-For Model 6, K''_{IBuOH}, K''_{IW}, K''_{BuOH}, K_2, K'_W and K_3 were neglected.

By discarding these parameters, the reduced models are displayed in Table 5. Table 6 is a summary of the modeling output for the different models. SSR is the sum of squared residuals, the difference between the experimental and simulated concentrations. AIC values showed that Model 4 is the most probable one (Table 4). Due to space limitation of the journal, the modeling results of the other models are displayed in Supporting Information (S5).

Table 5. Reduced kinetic models for the esterification of levulinic acid over immobilized enzyme.

Model	Kinetic term	Denominator
Model 1	$k_{Esterification} \cdot \rho_{Enzyme}$	1
Model 2	$k_f \cdot \rho_{Enzyme}$	$[LA] \cdot [BuOH] + K_{BuOH} \cdot [LA] + K_{LA} \cdot [BuOH]$
Model 3	$k_f \cdot \rho_{Enzyme}$	$[LA] \cdot [BuOH] + K_{BuOH} \cdot [LA] + K''_{IBuOH} \cdot [BuOH]^2 + K_{Lump} \cdot [W] \cdot [BL]$
Model 4	$k_f \cdot \rho_{Enzyme}$	$[LA] \cdot [BuOH] + K''_{ILA} \cdot [LA]^2 + K''_{IBuOH} \cdot [BuOH]^2 + K''_{BuOH-W} \cdot [W] \cdot [BuOH]$
Model 5	$k_{LA} \cdot \rho_{Enzyme}$	$K''_{BuOH} \cdot [BuOH] \cdot [LA] + [BuOH]$
Model 6	$k_{LA} \cdot \rho_{Enzyme}$	$K_1 \cdot [LA] + ([BuOH]) \cdot (1 + K''_{siBuOH} \cdot [BuOH]) \cdot (1 + K''_{siW} \cdot [W])$

Table 6. Modeling results for each Model.

	Model 1	Model 2	Model 3	Model 4	Model 5	Model 6
SSR	15.85	15.16	14.83	13.66	15.48	14.03
Number of estimated parameters	2	4	5	5	3	5
AIC	-2311.47	-2335.50	-2347.36	-2398.81	-2324.11	-2381.86

Table 7 shows the estimated values with their confidence intervals. One can notice that the confidence intervals for $ln\left(k_c(T_{ref})\right)$, $\frac{E_a}{R \cdot T_{ref}}$ and K''_{ILA} are small, meaning that the initial operating condition variation was well designed to estimate these parameters. Based on our experimental data, it was not possible to calculate the credible interval for K''_{IBuOH}, the optimum value was 51.52 mol.L^{-1}.

Table 7 presents the Normalized parameter covariance matrix for Model 4. According to Toch et al. [71], two parameters are correlated if their binary correlation coefficient is higher than 0.95. From Table 8, one can notice that the estimated parameters are not correlated.

Fig. 7 shows that the residuals, $[BL]_{exp,u} - [BL]_{sim,u}$, are randomly distributed versus the experimental concentration of BL ($[BL]_{exp,u}$) and the simulated by Model 4 ($[BL]_{sim,u}$). This means that there are no trends pertaining to the errors.

Fig. 8 shows the parity plot, and one can notice that Model 4 can predict the experimental data correctly.

Figs 9 show the fit of model 4 to some experimental concentrations of BL with the 95% prediction intervals and the mean estimated values. From Figs 9, one can notice that Model 4 fits well the experimental concentrations, and most of the experimental concentrations lie between the intervals. The fact that some experimental concentration points, in the majority at the beginning, are outside the prediction intervals can be because the LA dissociation is not considered in the modeling or the adsorption and inhibition terms were not correctly defined.

However, the fit of Model 4 to experimental concentration for experiments carried out with a molar ratio LA/BuOH: 1:1 is lower near to the equilibrium than for the other ratio.

This observation is because the equilibrium constant predicted by ePC-SAFT is less reliable for this ratio.

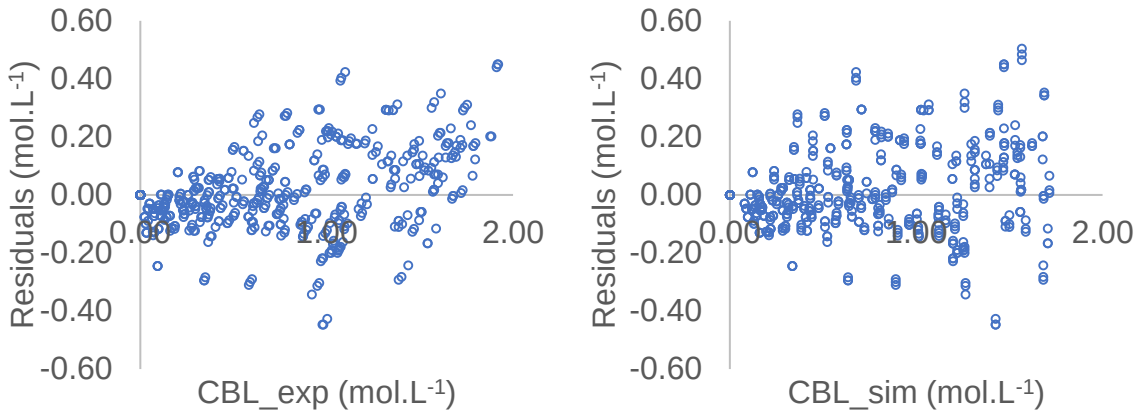

Fig. 7. Residual plots for Model 4.

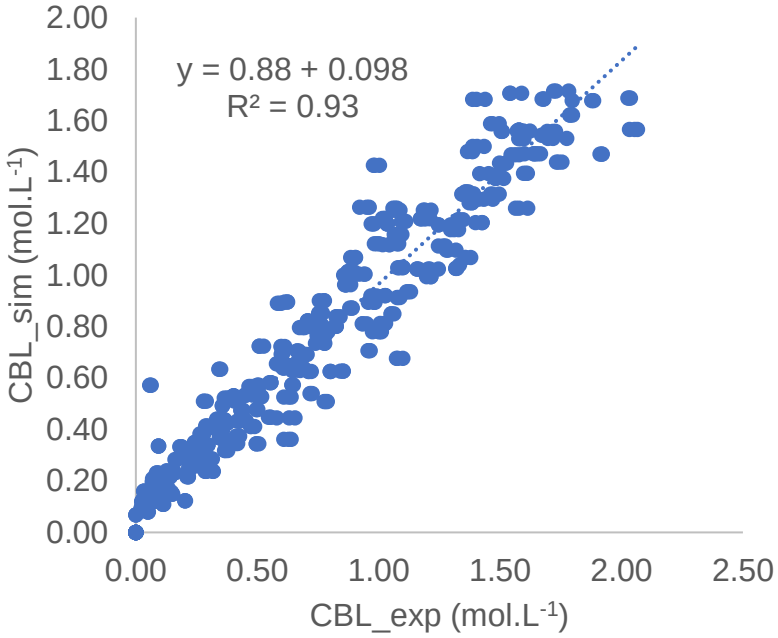

Fig. 8. Parity plot for Model 4.

Table 7. Estimated values at T_{ref} = 51°C and statistical data for Model 4.

	Units	Estimates	HPD%
$\ln\left(k_f(T_{ref})\right)$	mol·g^{-1}·min^{-1}	-2.02	6.25
$\frac{Ea_f}{R \cdot T_{ref}}$	-	11.01	5.56
K''_{ILA}	mol·L^{-1}	109.80	19.60
K''_{IBuOH}	mol·L^{-1}	51.52	
K''_{BuOH-W}	L·mol^{-1}	148.65	45.13

Table 8. Normalized parameter covariance matrix for Model 4.

	$\ln\left(k_f(T_{ref})\right)$	$\frac{Ea_f}{R \cdot T_{ref}}$	K''_{ILA}	K''_{BuOH-W}
$\ln\left(k_f(T_{ref})\right)$	1			
$\frac{Ea_f}{R \cdot T_{ref}}$	0.1	1		
K''_{ILA}	0.69	0.09	1	
K''_{BuOH-W}	0.93	0.12	0.53	1

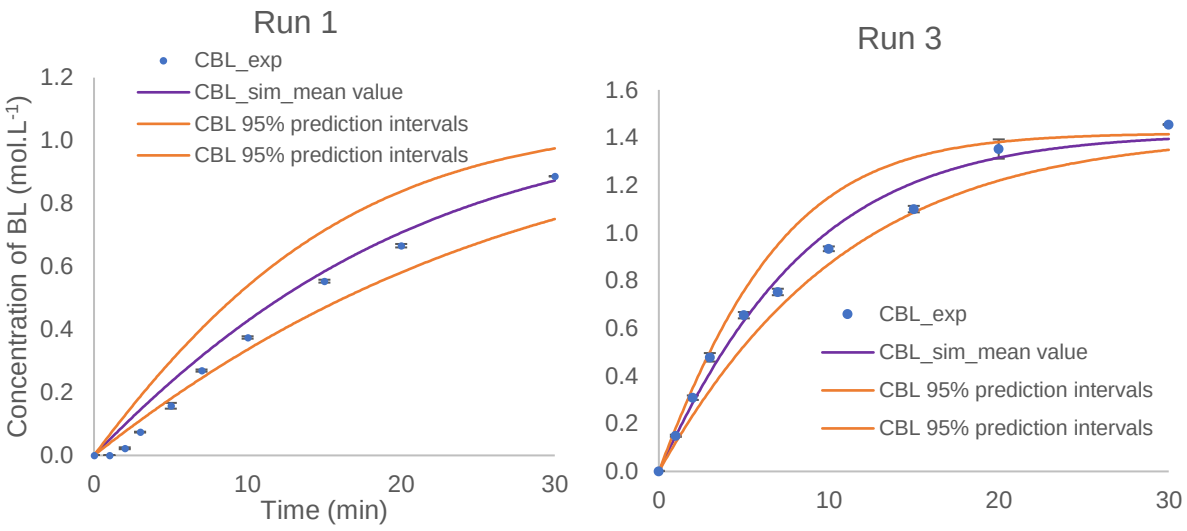

430

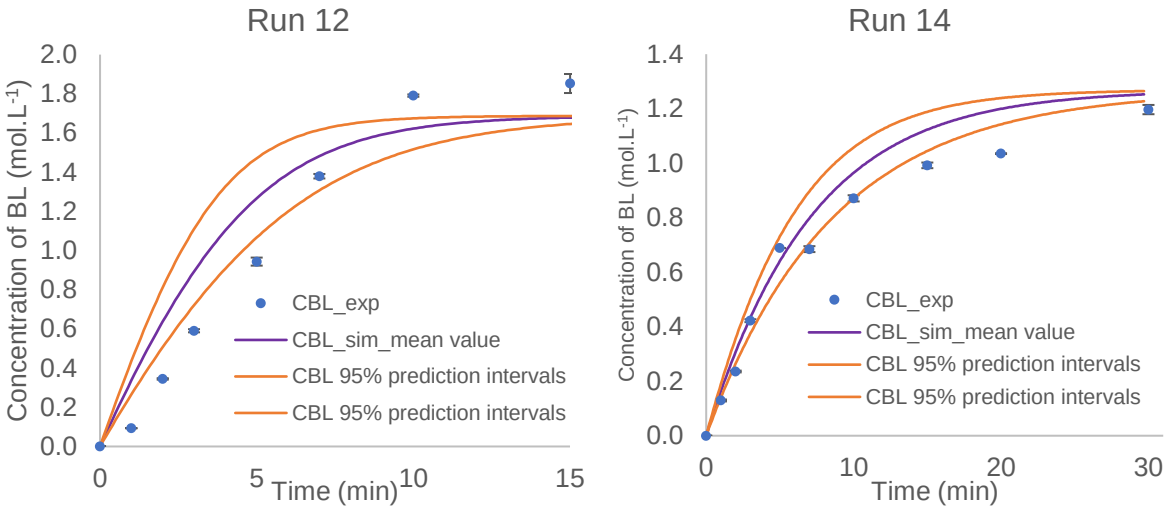

431

432

433

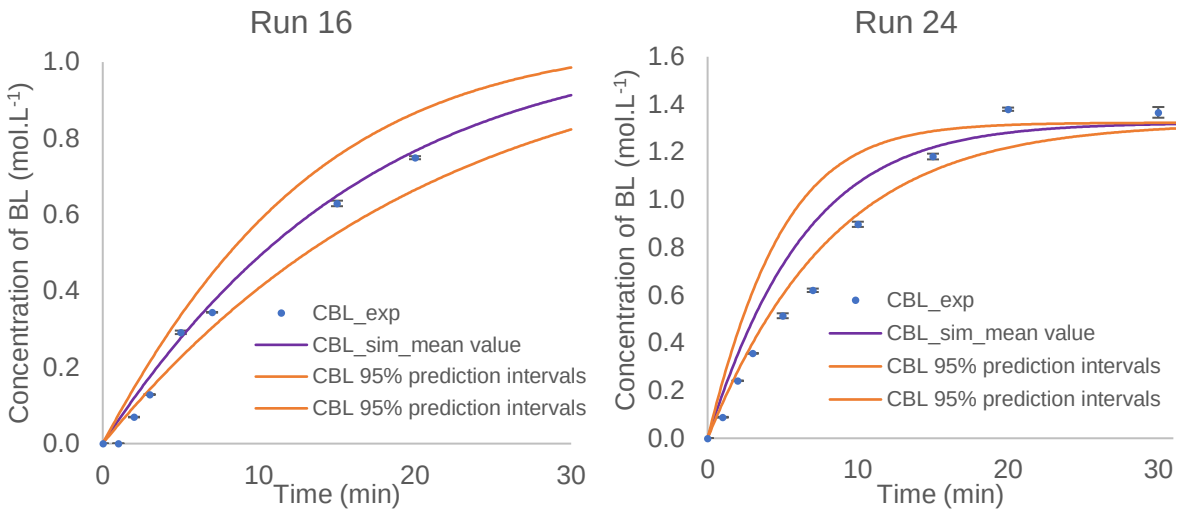

434

435 Fig. 9. Fit of Model 4 to the experimental concentrations with 95% prediction
436 intervals: experimental concentration of BL (blue circle), error bars (black), simulated
437 concentration of BL using the mean estimated value from Table 7 (purple line),
438 simulated concentration of BL using the estimated values at the extreme of the
439 confidence intervals from Table 7 (orange lines).

440

5. **Conclusions**

The synthesis of butyl levulinate from the esterification of levulinic acid over Novozym®435, an immobilized enzyme, was investigated in microfluidic technology in isothermal conditions. The enzyme's catalytic activity was found to be stable for 400 minutes. The internal and external mass transfer resistance was found to be negligible. Thus, a plug-flow model was used to estimate the kinetic constants.

Several kinetic experiments were performed by varying the reaction temperature from 20 to 80 °C, inlet LA concentration from 1.74 to 5.09 $mol.L^{-1}$, inlet butanol concentration from 5.09 to 9.07 $mol.L^{-1}$, mass of dried enzyme from 50 to 150 mg and residence time from 1 to 30 minutes.

The equilibrium constants were evaluated via the ePC-SAFT equation of state.

We evaluated 6 kinetic models based on power law, the classical Ping-Pong Bi-Bi mechanism and the modified one developed by Mitchell and Krieger. Based on the Akaike information criterion, we found that the classical Ping-Pong model, including the inhibition mechanism by butanol and levulinic acid, can fit the experimental concentrations properly. This model can reasonably predict the experimental concentration by considering the temperature effect on the rate constant.

Declaration of Competing Interest

The authors declare that they have no known competing financial interests or personal relationships that could have appeared to influence the work reported in this paper.

Acknowledgments

The authors thank INSA Rouen Normandy, University of Rouen Normandy, the Centre National de la Recherche Scientifique (CNRS), European Regional Development Fund (ERDF) N◦ HN0001343, Labex SynOrg (ANR-11-LABX-0029), Carnot Institute I2C, the graduate school for reasearch XL-Chem (ANR-18-EURE-0020 XL CHEM) and Region Normandie for their support. This research was funded, in whole or in part, by the ANR (French National Research Agency) and the DFG (German Research Foundation) through the project MUST (MicroflUidics for Structure-reactivity relationships aided by Thermodynamics & kinetics) [ANR-20-CE92-0002 & Project number 446436621].

References

[1] M.S. Singhvi, D. V. Gokhale, Lignocellulosic biomass: Hurdles and challenges in its valorization, Appl. Microbiol. Biotechnol. 103 (2019) 9305–9320. https://doi.org/10.1007/s00253-019-10212-7.

[2] Y.N. Guragain, P. V. Vadlani, Renewable Biomass Utilization: A Way Forward to Establish Sustainable Chemical and Processing Industries, Clean Technol. 3 (2021) 243–259. https://doi.org/10.3390/cleantechnol3010014.

[3] P. Zhu, O.Y. Abdelaziz, C.P. Hulteberg, A. Riisager, New synthetic approaches to biofuels from lignocellulosic biomass, Curr. Opin. Green Sustain. Chem. 21 (2020) 16–21. https://doi.org/10.1016/j.cogsc.2019.08.005.

[4] X. Lu, L. Lagerquist, K. Eränen, J. Hemming, P. Eklund, L. Estel, S. Leveneur, H. Grénman, Reductive Catalytic Depolymerization of Semi-industrial Wood-Based Lignin, Ind. Eng. Chem. Res. (2021) acs.iecr.1c03154. https://doi.org/10.1021/acs.iecr.1c03154.

[5] W. Schutyser, T. Renders, S. Van Den Bosch, S.F. Koelewijn, G.T. Beckham, B.F. Sels, Chemicals from lignin: an interplay of lignocellulose fractionation, depolymerisation, and upgrading, Chem. Soc. Rev. 47 (2018) 852–908. https://doi.org/10.1039/C7CS00566K.

[6] R. Rinaldi, R. Jastrzebski, M.T. Clough, J. Ralph, M. Kennema, P.C.A. Bruijnincx, B.M. Weckhuysen, Paving the Way for Lignin Valorisation: Recent Advances in Bioengineering, Biorefining and Catalysis, Angew. Chemie Int. Ed. 55 (2016) 8164–8215. https://doi.org/10.1002/ANIE.201510351.

[7] K.C. Badgujar, V.C. Badgujar, B.M. Bhanage, A review on catalytic synthesis of

energy rich fuel additive levulinate compounds from biomass derived levulinic acid, Fuel Process. Technol. 197 (2020) 106213. https://doi.org/10.1016/j.fuproc.2019.106213.

[8] D. Di Menno Di Bucchianico, Y. Wang, J.-C. Buvat, Y. Pan, V. Casson Moreno, S. Leveneur, Production of levulinic acid and alkyl levulinates: a process insight, Green Chem. 24 (2022) 614–646. https://doi.org/10.1039/d1gc02457d.

[9] A. Démolis, N. Essayem, F. Rataboul, Synthesis and applications of alkyl levulinates, ACS Sustain. Chem. Eng. 2 (2014) 1338–1352. https://doi.org/10.1021/sc500082n.

[10] L. Yan, Q. Yao, Y. Fu, Conversion of levulinic acid and alkyl levulinates into biofuels and high-value chemicals, Green Chem. 19 (2017) 5527–5547. https://doi.org/10.1039/c7gc02503c.

[11] Y. Wang, M. Cipolletta, L. Vernières-Hassimi, V. Casson-Moreno, S. Leveneur, Application of the concept of Linear Free Energy Relationships to the hydrogenation of levulinic acid and its corresponding esters, Chem. Eng. J. 374 (2019) 822–831. https://doi.org/10.1016/j.cej.2019.05.218.

[12] S. Capecci, Y. Wang, V. Casson Moreno, C. Held, S. Leveneur, Solvent effect on the kinetics of the hydrogenation of n-butyl levulinate to γ-valerolactone, Chem. Eng. Sci. 231 (2021) 116315. https://doi.org/10.1016/j.ces.2020.116315.

[13] D.M. Alonso, S.G. Wettstein, J.A. Dumesic, Gamma-valerolactone, a sustainable platform molecule derived from lignocellulosic biomass, Green Chem. 15 (2013) 584–595. https://doi.org/10.1039/C3GC37065H.

[14] L. Negahdar, M.G. Al-Shaal, F.J. Holzhäuser, R. Palkovits, Kinetic analysis of the catalytic hydrogenation of alkyl levulinates to γ-valerolactone, Chem. Eng. Sci. (2017). https://doi.org/10.1016/j.ces.2016.11.007.

[15] W.R.H. Wright, R. Palkovits, Development of heterogeneous catalysts for the conversion of levulinic acid to γ-valerolactone, ChemSusChem. 5 (2012) 1657–1667. https://doi.org/10.1002/cssc.201200111.

[16] S. Capecci, Y. Wang, J. Delgado, V. Casson Moreno, M. Mignot, H. Grénman, D.Y. Murzin, S. Leveneur, Bayesian Statistics to Elucidate the Kinetics of γ-Valerolactone from n-Butyl Levulinate Hydrogenation over Ru/C, Ind. Eng. Chem. Res. 60 (2021) 11725–11736. https://doi.org/10.1021/acs.iecr.1c02107.

[17] J. Delgado, W.N. Vasquez Salcedo, G. Bronzetti, V. Casson Moreno, M. Mignot, J. Legros, C. Held, H. Grénman, S. Leveneur, Kinetic model assessment for the synthesis of γ-valerolactone from n-butyl levulinate and levulinic acid hydrogenation over the synergy effect of dual catalysts Ru/C and Amberlite IR-120, Chem. Eng. J. 430 (2022) 133053. https://doi.org/10.1016/j.cej.2021.133053.

[18] L. Peng, X. Gao, K. Chen, Catalytic upgrading of renewable furfuryl alcohol to alkyl levulinates using AlCl3 as a facile, efficient, and reusable catalyst, Fuel. 160 (2015) 123–131. https://doi.org/10.1016/J.FUEL.2015.07.086.

[19] A.F. Peixoto, R. Ramos, M.M. Moreira, O.S.G.P. Soares, L.S. Ribeiro, M.F.R. Pereira, C. Delerue-Matos, C. Freire, Production of ethyl levulinate fuel bioadditive from 5-hydroxymethylfurfural over sulfonic acid functionalized biochar catalysts, Fuel. 303 (2021) 121227. https://doi.org/10.1016/J.FUEL.2021.121227.

[20] E. Christensen, A. Williams, S. Paul, S. Burton, R.L. McCormick, Properties and Performance of Levulinate Esters as Diesel Blend Components, Energy and Fuels. 25 (2011) 5422–5428. https://doi.org/10.1021/EF201229J.

[21] S. Frigo, G. Pasini, G. Caposciutti, M. Antonelli, A.M.R. Galletti, S. Gori, R. Costi, L. Arnone, Utilisation of advanced biofuel in CI internal combustion engine, Fuel. 297 (2021) 120742. https://doi.org/10.1016/J.FUEL.2021.120742.

[22] D. Di Menno Di Bucchianico, J.C. Buvat, M. Mignot, V. Casson Moreno, S. Leveneur, Role of solvent the production of butyl levulinate from fructose, Fuel. 318 (2022) 123703. https://doi.org/10.1016/j.fuel.2022.123703.

[23] A. Harwardt, K. Kraemer, B. Rüngeler, W. Marquardt, Conceptual Design of a Butyl-levulinate Reactive Distillation Process by Incremental Refinement, Chinese J. Chem. Eng. 19 (2011) 371–379. https://doi.org/10.1016/S1004-9541(09)60223-8.

[24] V. Russo, R. Tesser, C. Rossano, T. Cogliano, R. Vitiello, S. Leveneur, M. Di Serio, Kinetic study of Amberlite IR120 catalyzed acid esterification of levulinic acid with ethanol: From batch to continuous operation, Chem. Eng. J. 401 (2020) 126126. https://doi.org/10.1016/J.CEJ.2020.126126.

[25] M.A. Tejero, E. Ramírez, C. Fité, J. Tejero, F. Cunill, Esterification of levulinic acid with butanol over ion exchange resins, Appl. Catal. A Gen. 517 (2016) 56–66. https://doi.org/10.1016/J.APCATA.2016.02.032.

[26] A.F. Peixoto, S.M. Silva, P. Costa, A.C. Santos, B. Valentim, J.M. Lázaro-Martínez, C. Freire, Acid functionalized coal fly ashes: New solid catalysts for levulinic acid esterification, Catal. Today. 357 (2020) 74–83. https://doi.org/10.1016/j.cattod.2019.07.038.

[27] S. Dharne, V. V. Bokade, Esterification of levulinic acid to n-butyl levulinate over heteropolyacid supported on acid-treated clay, J. Nat. Gas Chem. 20 (2011) 18–24. https://doi.org/10.1016/S1003-9953(10)60147-8.

[28] K.Y. Nandiwale, V. V. Bokade, Esterification of Renewable Levulinic Acid to n-Butyl Levulinate over Modified H-ZSM-5, Chem. Eng. Technol. 38 (2015) 246–252. https://doi.org/10.1002/ceat.201400326.

[29] K.Y. Nandiwale, V. V. Bokade, Environmentally benign catalytic process for esterification of renewable levulinic acid to various alkyl levulinates biodiesel, Environ. Prog. Sustain. Energy. 34 (2015) 795–801. https://doi.org/10.1002/ep.12042.

[30] K.C. Maheria, J. Kozinski, A. Dalai, Esterification of Levulinic Acid to n-Butyl Levulinate Over Various Acidic Zeolites, Catal. Lett. 2013 14311. 143 (2013) 1220–1225. https://doi.org/10.1007/S10562-013-1041-3.

[31] M. Song, X. Di, Y. Zhang, Y. Sun, Z. Wang, Z. Yuan, Y. Guo, The effect of enzyme loading, alcohol/acid ratio and temperature on the enzymatic esterification of levulinic acid with methanol for methyl levulinate production: A kinetic study, RSC Adv. 11 (2021) 15054–15059. https://doi.org/10.1039/d1ra01780b.

[32] G.D. Yadav, I. V. Borkar, Kinetic Modeling of Immobilized Lipase Catalysis in Synthesis of n-Butyl Levulinate†, Ind. Eng. Chem. Res. 47 (2008) 3358–3363. https://doi.org/10.1021/IE800193F.

[33] V.N. Emel'yanenko, E. Altuntepe, C. Held, A.A. Pimerzin, S.P. Verevkin, Renewable platform chemicals: Thermochemical study of levulinic acid esters, Thermochim. Acta. 659 (2018) 213–221.

https://doi.org/10.1016/j.tca.2017.12.006.

[34] K. V. Bhavsar, G.D. Yadav, n-Butyl levulinate synthesis using lipase catalysis: comparison of batch reactor versus continuous flow packed bed tubular microreactor, J. Flow Chem. 8 (2018) 97–105. https://doi.org/10.1007/s41981-018-0014-5.

[35] L. Zhou, Y. He, L. Ma, Y. Jiang, Z. Huang, L. Yin, J. Gao, Conversion of levulinic acid into alkyl levulinates: Using lipase immobilized on meso-molding three-dimensional macroporous organosilica as catalyst, Bioresour. Technol. 247 (2018) 568–575. https://doi.org/10.1016/J.BIORTECH.2017.08.134.

[36] S. Zhai, L. Zhang, X. Zhao, Q. Wang, Y. Yan, C. Li, X. Zhang, Enzymatic synthesis of a novel solid–liquid phase change energy storage material based on levulinic acid and 1,4-butanediol, Bioresour. Bioprocess. 9 (2022) 1–10. https://doi.org/10.1186/s40643-022-00502-w.

[37] K.C. Badgujar, V.C. Badgujar, B.M. Bhanage, Lipase as a green and sustainable material for production of levulinate compounds: State of the art, Mater. Sci. Energy Technol. (2022). https://doi.org/10.1016/j.mset.2022.02.005.

[38] R. Gérardy, D.P. Debecker, J. Estager, P. Luis, J.C.M. Monbaliu, Continuous Flow Upgrading of Selected C2–C6 Platform Chemicals Derived from Biomass, Chem. Rev. 120 (2020) 7219–7347. https://doi.org/10.1021/ACS.CHEMREV.9B00846.

[39] H. Zhang, Y. Bai, N. Zhu, J. Xu, Microfluidic reactor with immobilized enzyme-from construction to applications: A review, Chinese J. Chem. Eng. 30 (2021) 136–145. https://doi.org/10.1016/J.CJCHE.2020.12.011.

[40] C.J. Taylor, J.A. Manson, G. Clemens, B.A. Taylor, T.W. Chamberlain, R.A. Bourne, Modern advancements in continuous-flow aided kinetic analysis, React. Chem. Eng. (2022). https://doi.org/10.1039/d1re00467k.

[41] H. Hajifatheali, E. Ahmadi, A. Wojtczak, Z. Jaglicic, The synthesis of N-methylbis[2-(dodecylthio)ethyl]amine (SNS) and investigation of its efficiency as new mononuclear catalyst complex in copper-based ATRP, Macromol. Res. 2015 2311. 23 (2015) 977–985. https://doi.org/10.1007/S13233-015-3132-Z.

[42] L.K. Doraiswamy, D.G. Tajbl, Laboratory Catalytic Reactors, Catal. Rev. 10 (1974) 177–219. https://doi.org/10.1080/01614947408079629.

[43] J.-M. Commenge, M. Saber, L. Falk, Methodology for multi-scale design of isothermal laminar flow networks, Chem. Eng. J. 173 (2011) 541–551. https://doi.org/10.1016/J.CEJ.2011.07.060.

[44] A.A. Hassankiadeh, Dynamic Assessment and Optimization of Catalytic Hydroprocessing Process: Sensitivity Analysis and Practical Tips, University of Newfoundland, 2021.

[45] S. Leveneur, J. Wärnå, K. Eränen, T. Salmi, Green process technology for peroxycarboxylic acids: Estimation of kinetic and dispersion parameters aided by RTD measurements: Green synthesis of peroxycarboxylic acids, Chem. Eng. Sci. 66 (2011) 1038–1050. https://doi.org/10.1016/j.ces.2010.12.005.

[46] J. Villermaux, Génie de la réaction chimique, Technip, Tec & Doc Lavoisier, Paris, 1993. http://www.lavoisier.fr/livre/notice.asp?depuis=e.lavoisier.fr&id=9782852067592.

[47] M. Ravelo, M. Wojtusik, M. Ladero, F. García-Ochoa, Synthesis of ibuprofen monoglyceride in solventless medium with novozym®435: Kinetic analysis, Catalysts. 10 (2020) 76. https://doi.org/10.3390/catal10010076.

[48] C.R. Wilke, P. Chang, Correlation of diffusion coefficients in dilute solutions, AIChE J. 1 (1955) 264–270. https://doi.org/10.1002/aic.690010222.

[49] H. Ariba, Y. Wang, C. Devouge-Boyer, R.P. Stateva, S. Leveneur, Physicochemical Properties for the Reaction Systems: Levulinic Acid, Its Esters, and γ-Valerolactone, J. Chem. Eng. Data. 65 (2020) 3008–3020. https://doi.org/10.1021/acs.jced.9b00965.

[50] D.M. Chesterfield, P.L. Rogers, E.O. Al-Zaini, A.A. Adesina, Production of biodiesel via ethanolysis of waste cooking oil using immobilised lipase, Chem. Eng. J. 207–208 (2012) 701–710. https://doi.org/10.1016/J.CEJ.2012.07.039.

[51] C. Ortiz, M.L. Ferreira, O. Barbosa, J.C.S. Dos Santos, R.C. Rodrigues, Á. Berenguer-Murcia, L.E. Briand, R. Fernandez-Lafuente, Novozym 435: The “perfect” lipase immobilized biocatalyst?, Catal. Sci. Technol. 9 (2019) 2380–2420. https://doi.org/10.1039/c9cy00415g.

[52] D. Kowalczykiewicz, K. Szymańska, D. Gillner, A.B. Jarzębski, Rotating bed reactor packed with heterofunctional structured silica-supported lipase. Developing an effective system for the organic solvent and aqueous phase reactions, Microporous Mesoporous Mater. 312 (2021) 110789. https://doi.org/10.1016/j.micromeso.2020.110789.

[53] H. Zhao, Z. Song, Migration of reactive trace compounds from Novozym® 435 into organic solvents and ionic liquids, Biochem. Eng. J. 49 (2010) 113–118. https://doi.org/10.1016/j.bej.2009.12.004.

660 [54] J. Gross, G. Sadowski, Perturbed-Chain SAFT: An Equation of State Based on
661 a Perturbation Theory for Chain Molecules, Ind. Eng. Chem. Res. 40 (2001)
662 1244–1260. https://doi.org/10.1021/IE0003887.

663 [55] M. Lemberg, G. Sadowski, Predicting the Solvent Effect on Esterification
664 Kinetics, ChemPhysChem. 18 (2017) 1977–1980.
665 https://doi.org/10.1002/cphc.201700507.

666 [56] E. Altuntepe, V.N. Emel'yanenko, M. Forster-Rotgers, G. Sadowski, S.P.
667 Verevkin, C. Held, Thermodynamics of enzyme-catalyzed esterifications: II.
668 Levulinic acid esterification with short-chain alcohols, Appl. Microbiol.
669 Biotechnol. 101 (2017) 7509–7521. https://doi.org/10.1007/s00253-017-8481-
670 4.

671 [57] C. Held, G. Sadowski, Thermodynamics of Bioreactions, Annu. Rev. Chem.
672 Biomol. Eng. 7 (2016) 395–414. https://doi.org/10.1146/annurev-chembioeng-
673 080615-034704.

674 [58] F. Tumakaka, G. Sadowski, Application of the Perturbed-Chain SAFT equation
675 of state to polar systems, in: Fluid Phase Equilib., American Chemical Society,
676 2004: pp. 233–239. https://doi.org/10.1016/j.fluid.2002.12.002.

677 [59] D. Fuchs, J. Fischer, F. Tumakaka, G. Sadowski, Solubility of Amino Acids:
678 Influence of the pH value and the Addition of Alcoholic Cosolvents on Aqueous
679 Solubility, Ind. Eng. Chem. Res. 45 (2006) 6578–6584.
680 https://doi.org/10.1021/IE0602097.

681 [60] G.D. Yadav, S. V. Pawar, Synergism between microwave irradiation and
682 enzyme catalysis in transesterification of ethyl-3-phenylpropanoate with n-
683 butanol, Bioresour. Technol. 109 (2012) 1–6.

https://doi.org/10.1016/j.biortech.2012.01.030.

[61] S.R. Bansode, M.A. Hardikar, V.K. Rathod, Evaluation of reaction parameters and kinetic modelling for Novozym 435 catalysed synthesis of isoamyl butyrate, J. Chem. Technol. Biotechnol. 92 (2017) 1306–1314. https://doi.org/10.1002/jctb.5125.

[62] S.A. Zulkeflee, S.A. Sata, F.S. Rohman, N. Aziz, Modelling of immobilized Candida rugosa lipase catalysed esterification process in batch reactor equipped with temperature and water activity control system, Biochem. Eng. J. 161 (2020) 107669. https://doi.org/10.1016/j.bej.2020.107669.

[63] D.A. Mitchell, N. Krieger, Looking through a new lens: Expressing the Ping Pong bi bi equation in terms of specificity constants, Biochem. Eng. J. 178 (2022) 108276. https://doi.org/10.1016/j.bej.2021.108276.

[64] C.G. Lopresto, V. Calabrò, J.M. Woodley, P. Tufvesson, Kinetic study on the enzymatic esterification of octanoic acid and hexanol by immobilized Candida antarctica lipase B, J. Mol. Catal. B Enzym. 110 (2014) 64–71. https://doi.org/10.1016/j.molcatb.2014.09.011.

[65] M.N. Varma, G. Madras, Kinetics of synthesis of butyl butyrate by esterification and transesterification in supercritical carbon dioxide, J. Chem. Technol. Biotechnol. 83 (2008) 1135–1144. https://doi.org/10.1002/jctb.1897.

[66] M. Rizzi, P. Stylos, A. Riek, M. Reuss, A kinetic study of immobilized lipase catalysing the synthesis of isoamyl acetate by transesterification in n-hexane, Enzyme Microb. Technol. 14 (1992) 709–714. https://doi.org/10.1016/0141-0229(92)90110-A.

[67] M. Caracotsios, W.E. Stewart, Sensitivity analysis of initial value problems with mixed odes and algebraic equations, Comput. Chem. Eng. 9 (1985) 359–365. https://doi.org/10.1016/0098-1354(85)85014-6.

[68] W.E. Stewart, M. Caracotsios, Computer-Aided Modeling of Reactive Systems, First, New Jersey, 2008. https://doi.org/10.1002/9780470282038.

[69] G. Buzzi-Ferraris, Planning of experiments and kinetic analysis, Catal. Today. 52 (1999) 125–132. https://doi.org/10.1016/S0920-5861(99)00070-X.

[70] M.A. McDonald, L. Bromig, M.A. Grover, R.W. Rousseau, A.S. Bommarius, Kinetic model discrimination of penicillin G acylase thermal deactivation by non-isothermal continuous activity assay, Chem. Eng. Sci. 187 (2018) 79–86. https://doi.org/10.1016/j.ces.2018.04.046.

[71] K. Toch, J.W. Thybaut, G.B. Marin, A systematic methodology for kinetic modeling of chemical reactions applied to n-hexane hydroisomerization, AIChE J. 61 (2015) 880–892. https://doi.org/10.1002/aic.14680.